

NdN: An intrinsic ferromagnetic semiconductorE.-M. Anton,^{1,*} J. F. McNulty,¹ B. J. Ruck,¹ M. Suzuki,² M. Mizumaki,² V. N. Antonov,³ J. W. Quilty,⁴ N. Strickland,⁵ and H. J. Trodahl¹¹*MacDiarmid Institute for Advanced Materials and Nanotechnology, School of Chemical and Physical Sciences, Victoria University of Wellington, P.O. Box 600, Wellington 6140, New Zealand*²*Japan Synchrotron Radiation Research Institute (JASRI/SPring-8), 1-1-1 Kouto, Sayo, Hyogo 679-5198, Japan*³*Institute of Metal Physics, National Academy of Sciences of Ukraine, 03142 Kiev, Ukraine*⁴*School of Engineering and Computer Science, Victoria University of Wellington, P.O. Box 600, Wellington 6140, New Zealand*⁵*MacDiarmid Institute for Advanced Materials and Nanotechnology, Robinson Research Institute, Victoria University of Wellington, P.O. Box 33436, Lower Hutt 5046, New Zealand*

(Received 10 December 2015; published 26 February 2016)

The rare-earth nitrides have recently regained attention due to findings that most members of the series are intrinsic ferromagnetic semiconductors, a class of materials that is crucial for the development of spintronics devices. Here we present a study of NdN thin films, with films grown via molecular beam epitaxy. Optical transmission measurements revealed a band gap of about 0.9 eV, while resistivity measurements confirmed semiconducting behavior with a negative temperature coefficient of resistance, though semimetallic behavior could not be ruled out. The room temperature resistivity of 0.6 mΩ cm indicates strong doping by nitrogen vacancies. Magnetization measurements show a ferromagnetic moment of $1.0 \pm 0.2\mu_B$ below the Curie temperature T_C of 43 ± 1 K, strongly suppressed from the Hund's rules value of $3.27\mu_B$ per ion. The ferromagnetic moment is strongly quenched and the T_C is enhanced compared to previously studied bulk NdN, and crystal field calculations reveal that the quenched moment is likely due to lattice strain. X-ray magnetic circular dichroism measurements show that the magnetic moment is orbital dominant, placing NdN in the same category as SmN, an intrinsic ferromagnetic semiconductor with an orbital-dominant ferromagnetic moment.

DOI: [10.1103/PhysRevB.93.064431](https://doi.org/10.1103/PhysRevB.93.064431)**I. INTRODUCTION**

Over the past decade, the rare-earth nitrides have revealed a wide range of contrasting magnetic behaviors related to the strong spin-orbit interaction of the $4f$ shells. This is especially intriguing because most of the group are ferromagnetic semiconductors, which makes them promising materials for spintronic devices [1]. The strong spin-orbit coupling leads to an orbital contribution to the ferromagnetic moment that is not quenched by the crystal field. The orbital moment then enhances the net magnetic moment in the heavy rare earths, but for the elements lighter than Gd the orbital contribution reduces, and can even reverse, the net moment relative to the spin magnetic moment. In this situation the majority spin has an orientation opposite to that expected based on the conventional purely spin-magnetism scenario; they are examples of the so-called negative magnetization materials [2]. One particularly interesting material is SmN [3,4]. It has been theoretically predicted [5] and experimentally verified [4] that its spin and orbital moments have the opposite sign, with the orbital moment being only slightly larger than the spin moment. That means SmN is among the negative spin magnetization materials, but with a very small net magnetic moment. This spin/orbital alignment in SmN causes the surprising effect of a twisted magnetic phase when it is in contact with the spin-only ferromagnet GdN, similar to a field-tunable domain wall [6]. Larson *et al.* [5] predicted the same basic configuration of spin and orbital moments for NdN,

though in this case the orbital moment is clearly dominant. The resulting strong ferromagnetic net moment makes NdN an ideal model system to study magnetic materials with an orbital dominant magnetism. Similarly interesting effects to those seen in SmN are expected when incorporating NdN into heterojunction devices with GdN and other rare-earth nitrides.

The transport behavior of the rare-earth nitrides was not clearly established in the early studies of the 1960s and 1970s, mainly because of difficulties with oxygen contamination and nonstoichiometry. Modern studies using molecular beam epitaxy growth in ultrahigh vacuum chambers overcame those issues, such that high-quality thin films can now be produced [1]. For many members of the series there is now evidence for semiconducting behavior, namely, GdN [7], ErN [8], DyN [9], SmN [10], EuN [11], and YbN [12]. Very little information has been published on the conducting state of NdN. Sclar [13] reported the room temperature resistivity and temperature coefficient of resistance of polycrystalline NdN as 7.5 mΩ cm and $7 \times 10^{-4} \text{ K}^{-1}$, respectively, but they pointed out that grain scattering and oxidation in the pressed powders will have increased the resistivity. Sclar noted that the positive temperature coefficient indicates a metallic behavior, but could also result from a semiconductor heavily doped by nitrogen vacancies. The only optical study on NdN that the authors are aware of also gives hints that NdN has an optical band gap of 0.8 eV and might be a semiconductor, even though the samples were partly oxidized [14]. LSDA + U calculations predict a direct band gap of 0.76 eV and an indirect gap of 0.3 eV [5].

The Hund's rule ground state of Nd^{3+} is $L = 6$, $S = 3/2$, and $J = 9/2$. There is some experimental data available on the magnetic properties of NdN, but reports are still limited to

*eva.anton@vuw.ac.nz

TABLE I. Magnetic properties of NdN.

	Paramagnetic		Ferromagnetic	
	θ_p (K)	$m_{\text{eff}}(\mu_B)$	T_C (K)	$m_{\text{sat}}(\mu_B)$
NdN film (this study)	3 ± 4	3.6 ± 0.1	43 ± 1	1.0 ± 0.2
Free ion Nd^{3+} (Hund's rules)	–	3.62	–	3.27
Busch <i>et al.</i> [15,16], Junod <i>et al.</i> [19]	24	3.65–4.00	32	3.1
Schumacher and Wallace [17]	15	3.70	35	2.15
Olcese [18]	10	3.63		
Schobinger-Papamantellos [22] (neutron diffraction)				2.7
Veyssie <i>et al.</i> [21] (T_C from specific heat)	19	Eq. free ion	27.6	2.2
Mourgout <i>et al.</i> [31] ($\text{NdN}_{0.98}\text{O}_{0.02}$)	20/23	3.58/3.69	25/33.5	1.89/1.84

the early studies on bulk or powder samples of the 1960s and 1970s. So far no data on NdN thin films has been reported. Busch *et al.* [15,16] investigated the magnetic properties of bulk NdN, and found a paramagnetic Curie temperature $\theta_p = 24$ K, Curie temperature $T_C = 32$ K, effective paramagnetic moment in the range $m_{\text{eff}} = 3.65\text{--}4.00\mu_B$ and a spontaneous ferromagnetic magnetization of $3.1\mu_B$. Schumacher and Wallace [17] found $\theta_p = 15$ K, $T_C = 35$ K, and $m_{\text{eff}} = 3.70\mu_B$; Olcese [18] found $\theta_p = 10$ K and $m_{\text{eff}} = 3.63\mu_B$, and Junod *et al.* found [19] $\theta_p = 24$ K, $T_C = 32$ K, $m_{\text{eff}} = 3.5\text{--}4.0\mu_B$ and ferromagnetic saturation magnetization $m_{\text{sat}} = 3.1\mu_B$. Those reports also show the temperature-dependent data of the inverse susceptibility, and Junod *et al.* [19] additionally show magnetization measurements up to 80 kOe in pulsed fields. These are the only published datasets of magnetic measurements on NdN that could be accessed by the authors (see Table I). Ferromagnetic saturation moments were reported between 1.8 and $3.1\mu_B$ [20]. Veyssie *et al.* [21] measured $T_C = 27.6$ K in a specific heat study. Neutron diffraction experiments suggested a simple ferromagnetic structure in NdN [22]. The aim of this work is to revisit the magnetic, transport, and optical properties of NdN by an experimental study on ultrahigh vacuum grown thin films, supported by crystal-field and LSDA + U calculations.

II. METHODS

Thin NdN films were prepared by molecular beam epitaxy in a Thermionics ultrahigh vacuum chamber with a base pressure of 10^{-8} mbar. The substrates were bare c -plane sapphire and c -plane sapphire which was commercially coated with an epitaxial layer of $5\ \mu\text{m}$ GaN or $1\ \mu\text{m}$ AlN, called templated substrates hereafter. All substrates were outgassed at 360°C for 1.5 to 2 h before growth. During the growth the substrates were held at 400°C and rotated for better homogeneity. Nd metal was evaporated by an electron gun in the presence of high purity 3×10^{-4} mbar N_2 . The NdN forms spontaneously under these conditions. NdN behaves similarly to the other rare-earth nitrides in this respect, except for EuN and YbN, both of which have the propensity to form divalent ions and need activated nitrogen to form the nitride. The films were grown to about 120 nm thickness and capped with 50 nm GaN or AlN to prevent oxidation. Ga metal was evaporated by an electron gun and Al by an effusion cell under the same nitrogen pressure. In the case of the capping layers activated

nitrogen, obtained by a Kaufman ion source, is necessary for GaN or AlN to form.

X-ray diffraction (XRD) and x-ray reflectivity (XRR) patterns were taken with a PANalytical XPert Pro MPD, using Cu $K\alpha$ radiation. The XRR data was used to measure the thickness of the NdN films and capping layers. The resistivity measurements were performed with four electrical contacts using silver epoxy and copper wire in the van der Pauw geometry in a Quantum Design PPMS. Optical transmission data were obtained between 0.38 and 6.2 eV with a Perkin-Elmer Lambda 1050 spectrophotometer and independently with an FT-IR spectrometer (ABB Bomem DA8). Magnetic measurements with the magnetic field in the plane of the thin film were performed using a Quantum Design MPMS-7 SQUID magnetometer. Field-cooled (FC) and zero-field-cooled (ZFC) temperature-dependent magnetization were measured, where ZFC means that the sample was cooled without a field from room temperature to 5 K, then a small field of 25 mT was applied at low temperature and the magnetic moment was measured while warming in the applied field. In the FC measurements a field of 25 mT was applied at room temperature and measurements were taken while cooling in the applied field. X-ray absorption (XAS) and x-ray magnetic circular dichroism (XMCD) were measured at the beamline 39XU at the SPring-8 synchrotron in Japan. The x-ray propagation direction and magnetic field were collinear and at an angle of 18° from grazing incidence of the film. The detection method was partial fluorescence yield, which means only the $L_{\alpha 1}$ or $L_{\beta 1}$ fluorescence was measured at the Nd L_3 or L_2 edges, respectively. The XMCD data was normalized to the edge jump in XAS and corrected for an imbalance between left and right circularly polarized beams.

To guide the interpretation of our experimental data, XAS and XMCD spectra were calculated using the fully relativistic spin-polarized linear-muffin-tin-orbital method [23,24] within a local spin density approximation with Hubbard- U correction (LSDA + U) [25] with $U = 8$ eV. Details of the calculations can be found elsewhere [4,26,27].

III. RESULTS AND DISCUSSION

A. Structure, resistivity, and optical data

In Fig. 1 the XRD patterns for two NdN thin films are shown, with one grown on an AlN templated sapphire substrate, and the other sample on bare sapphire. For comparison

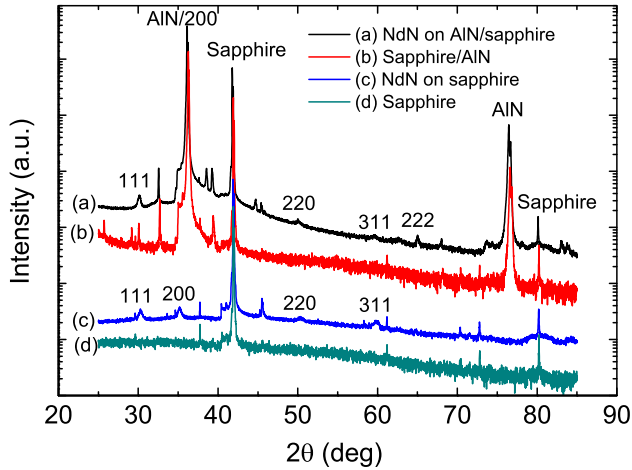


FIG. 1. XRD patterns for (a) a NdN thin film on AlN templated sapphire substrate next to (b) an AlN/sapphire substrate, and (c) a NdN thin film grown on a sapphire substrate next to (d) sapphire for comparison. The capping layer was GaN for both samples. The patterns are shifted along the vertical axis for clarity.

the corresponding substrate XRD patterns are also presented. The reflections originating from the thin films are consistent with the expected cubic rocksalt structure with a lattice constant of 5.137 Å, close to the literature value for bulk NdN of 5.132 Å [18]. This confirms that the produced layers were indeed NdN.

To investigate the transport properties of NdN the temperature-dependent resistivity of the thin films was measured with the results presented in Fig. 2. The resistivity varies from 0.6 mΩ cm at room temperature to nearly 1 mΩ cm at 3.5 K. The overall shape of the curve suggests semiconducting behavior, with a negative temperature coefficient of resistance and a steep upturn of resistivity at low temperatures. The room temperature resistivity is low for a semiconductor, but still orders of magnitude higher than in most metals. The

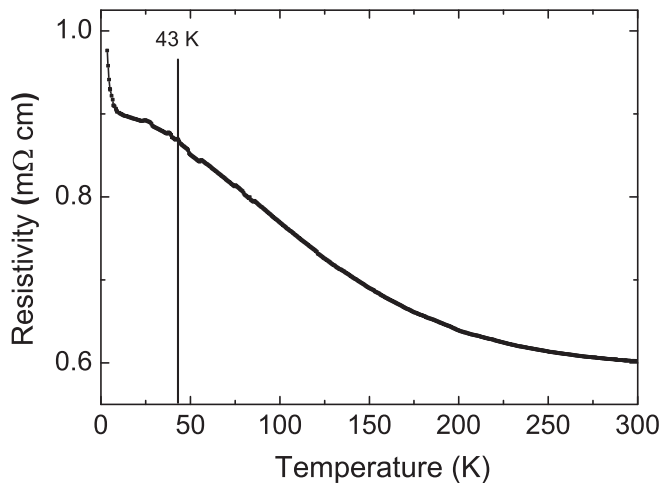


FIG. 2. Temperature-dependent resistivity of a NdN thin film capped with GaN, grown on a GaN templated sapphire substrate. The vertical line at 43 K denotes the T_c as obtained from the analysis of the magnetic data.

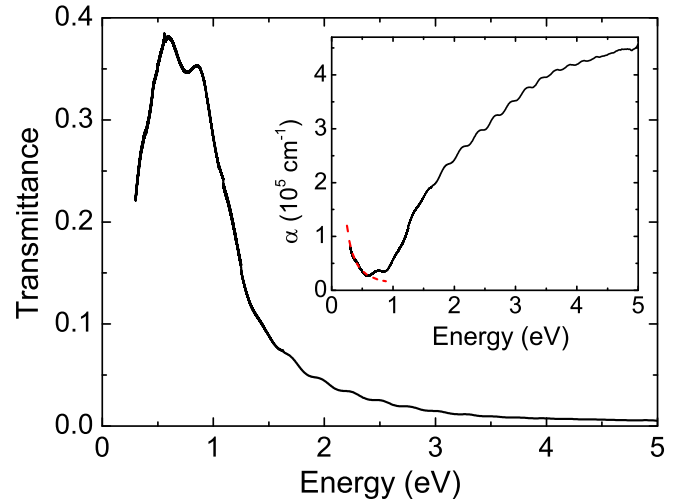


FIG. 3. Optical transmittance of a NdN film on an AlN/sapphire substrate capped with GaN. Inset: The absorption coefficient α as obtained from the transmittance after correction for the net reflectance of the interfaces. The red dashed line shows the Drude-model fit to the low-energy part of the absorption coefficient.

change of resistivity across the measured temperature range is comparably small, which indicates that the number of charge carriers is not strongly affected by the temperature. A fit of an activated conduction model above 100 K yields an activation energy of only 1 meV. These observations agree well with reports from other rare-earth nitrides, which are heavily n -doped by nitrogen vacancies [7,8,28]. Since this film was grown at high temperatures, a large number of nitrogen vacancies and thus charge carriers were expected [29,30] and we conclude that this NdN film is a heavily doped semiconductor. We note that at this stage a small band overlap cannot be ruled out and the studied NdN thin films could also have been semimetallic. The resistivity curve gives a first hint of the magnetic properties of the NdN thin films. There is an anomaly in the form of a broad hump around 40 K, which is associated with the onset of ferromagnetic ordering. The vertical line marks the T_c of 43 K, found by magnetic measurements reported below.

Optical transmittance (T_O) data in Fig. 3 show strong interband absorption above 1 eV. To determine the absorption coefficient it is necessary to correct for the net reflectance $R_O \sim 50\%$ from the interfaces across the sapphire/AlN/NdN/GaN stack. After that correction the absorption coefficient α is, to first order, $\alpha = \ln[T_O/(1 - R_O)/d]$, where d is the sample thickness, which is then shown in the inset of Fig. 3. Note that neither the reflection nor the transmittance were corrected for thin-film interference, so that relatively weak fringes remain in the inset. There is clear evidence of an interband absorption edge at ~ 0.9 eV, very close to the 0.8 eV predicted within an LSDA + U treatment [5]. The free carrier contribution leading to a rising absorption below 0.5 eV follows the Drude form $\sigma_{dc}/(\omega\tau)^2$ for a relaxation time τ of $\sim 10^{-14}$ s and a mean free path of order 5 nm. The carrier density then implied by the dc conductivity is $\sim 5 \times 10^{20}$ cm $^{-3}$, corresponding to the expected doping from a nitrogen vacancy concentration of $\sim 1\%$, as we commonly find in our rare-earth nitride films.

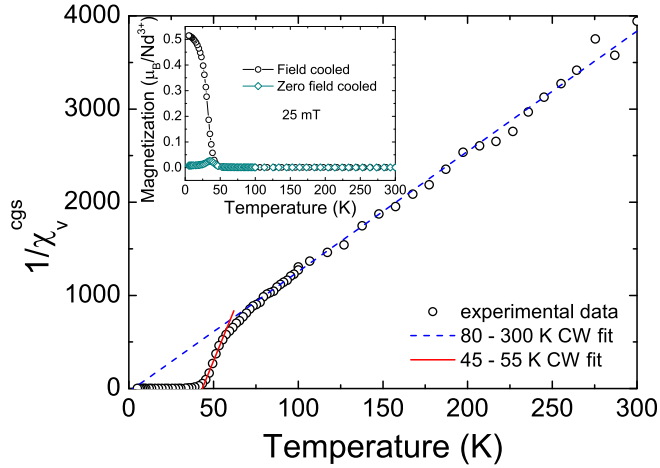


FIG. 4. Inverse susceptibility obtained from FC magnetization measurements on a NdN thin film grown on a sapphire substrate; the capping layer is AlN. Black circles are experimental data, the blue dashed line represents the high temperature, and the red solid line the low temperature Curie-Weiss fit. Inset: FC (black circles) and ZFC (green diamonds) temperature dependence of magnetization.

B. Magnetic properties

Figure 4 presents magnetic measurements on NdN thin films. The inset presents the FC and ZFC in-plane magnetization. The FC magnetization shows an upturn and subsequent saturation at low temperatures, giving a clear indication of ferromagnetism with a T_C below 50 K. The ZFC curve deviates from the FC curve around 43 K, which means at this point the applied field is smaller than the coercive field providing a lower limit on T_C . To analyze the data quantitatively, we performed a Curie-Weiss fit to the volume magnetic susceptibility χ according to

$$\chi = \frac{C}{T - \theta_p} + A, \quad (1)$$

with the Curie constant C , the temperature T , Curie point θ_p , and a temperature-independent contribution A , which is mainly due to the diamagnetic contribution of the substrate. While the fit was performed directly to χ with the free parameters C , θ_p , and A , it is useful to plot the inverse susceptibility $1/\chi$ with the substrate contribution A subtracted (main part of Fig. 4), because in this representation the slope of the linear fit corresponds to the inverse of C and the intersection with the horizontal axis denotes θ_p . It is immediately obvious that $1/\chi$ does not follow the Curie-Weiss law in the full temperature range above θ_p , but changes slope below about 70 K, and then again becomes linear below 55 K. We thus fit the data separately in a high temperature range between 80 and 300 K and in a low temperature range between 45 and 55 K.

The high temperature fit yields $C = 0.078 \pm 0.005$ K and $\theta_p = 3 \pm 4$ K, where C is given by $C = \frac{Nm_{\text{eff}}^2}{3k_B}$, with N the number of magnetic atoms per unit volume, Boltzmann constant k_B , and effective paramagnetic moment m_{eff} . Thus one can extract m_{eff} from the high temperature fit; we obtain $m_{\text{eff}} = 3.6 \pm 0.1\mu_B$. Our value is in good agreement with the experimental values reported in other studies, e.g., $3.63\mu_B$ by

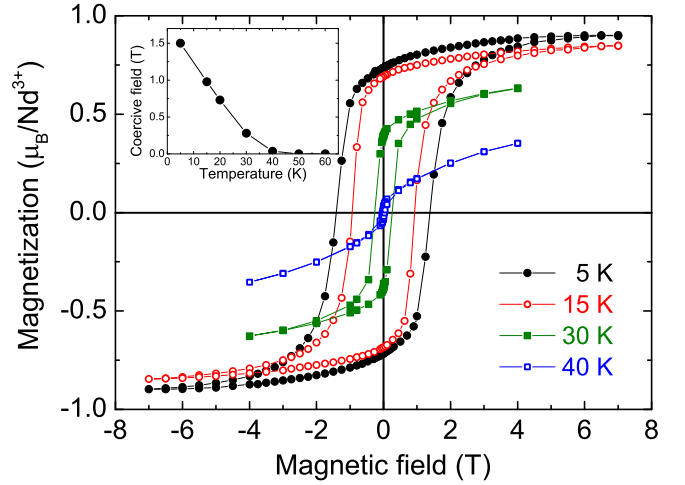


FIG. 5. Magnetic hysteresis loops of a NdN thin film capped with AlN at various temperatures. An identical diamagnetic contribution from the sapphire substrate has been subtracted from each dataset. Inset: Temperature dependence of the coercive field.

Olcese [18] and $3.70\mu_B$ by Schumacher and Wallace [17]. The m_{eff} calculated for the Hund's rules ground state of Nd^{3+} is given by $m_{\text{eff}} = g_j\mu_B\sqrt{J(J+1)}$ with the Landé g factor $g_j = 8/11$ and total angular momentum quantum number $J = 9/2$. The calculated values are then $m_{\text{eff}} = 3.62\mu_B$ and $C = 0.08$ K, in excellent agreement with the experiment. Magnetic properties of NdN films from this study, calculated free ion moments, and experimental literature values are listed in Table I.

The low temperature fit between 45 and 55 K on the other hand yields $C = 0.024 \pm 0.002$ K, $\theta_p = 43.2 \pm 0.2$ K, and $m_{\text{eff}} = 2.0 \pm 0.1\mu_B$. θ_p is in agreement with both the T_C as expected from the upturn of magnetization in the FC data and the vanishing hysteresis in the field-dependent magnetic measurements shown in the inset of Fig. 5. Taking into account the uncertainties of the selected fitting range, we quote $T_C = 43 \pm 1$ K for our NdN films. This value is significantly higher than the T_C 's between 27.6 and 35 K reported for bulk NdN [16,17,19,21].

It becomes clear that the high temperature range of $1/\chi$ can be well explained by the Curie-Weiss law and the obtained experimental effective moment is in excellent agreement with the expectation for a free Nd^{3+} ion. At lower temperatures, however, the effects of the crystal field become important and cause deviations from the Curie-Weiss law. It is known that under the influence of the crystal field the ground-state multiplet of Nd^{3+} splits into a doublet and two quartets [17,32]. Whereas at higher temperatures all energy levels are thermally occupied, the level population will change towards lower energy levels below about 80 K and for very low temperatures only the ground state will be occupied. Those changes in the population of the sublevels result in variations of the moment and thus deviations from the Curie-Weiss behavior. Those deviations from the Curie-Weiss behavior are also visible in the historical data for NdN [17]. A similar change in slope of $1/\chi$ towards lower temperatures has been observed for ErN and explained by crystal field effects by Meyer *et al.* [8].

Figure 5 shows the magnetic hysteresis loops for NdN measured up to 7 T at various temperatures after correction for the diamagnetic contribution of the substrate. The shape of the loops is typical for ferromagnetic materials and provides additional evidence for ferromagnetic behavior in the NdN thin film. These hysteresis loops show that NdN has a relatively large coercive field of 1.4 T at 5 K. The square shape of the loop with high remanent magnetization implies a simple magnetic structure, unlike the spiral structure found in some of the heavy rare-earth nitrides [8,33]. A simple magnetic structure is also in agreement with findings from neutron diffraction measurements [22]. The curve at the lowest temperature of 5 K saturates at $m_{\text{sat}} = 0.90 \pm 0.07\mu_B$. A different sample gave $1.04 \pm 0.12\mu_B$ in good agreement, and all other samples showed values in that range, but with larger uncertainties due to difficulties in the thickness measurements. Thus we quote an ordered moment of $1.0 \pm 0.2\mu_B$. The remanent magnetization is $0.74\mu_B$ and can be used to estimate the spontaneous moment. If the easy axis lies along one of the high symmetry directions then, in a polycrystalline sample, at remanence the moments will lie distributed within a cone of half-angle 54.7° around the magnetic field direction. The remanent magnetization is then reduced from the saturation value by about 15% [34], leading to an estimate of $m_{\text{sat}} = 0.86\mu_B$, in excellent agreement with the high field value.

In view of the moment being much less than the free ion moment $g_j\mu_B J = 3.27\mu_B$, it is essential to establish that all of the Nd ions participate in the ferromagnetic order, and that there are no ions in a paramagnetic phase. Indeed, there is no evidence for any phase other than NdN in the XRD spectra, but even more importantly, in a paramagnetic phase the Nd ions show a larger moment than we measure in the ferromagnetic state. Note that at the lowest temperature (5 K) and highest field (7 T) the ratio $m_{\text{eff}}B/k_B T = 3.1$ and in these conditions a paramagnetic phase approaches saturation. Such a paramagnetic phase would then be easily distinguished in the hysteresis data in Fig. 5, most clearly by a strong divergence between the 5 and 15 K magnetization. No such divergence exists, with an accuracy that ensures no more than 2% of the Nd ions are in any but the ferromagnetic phase. The resulting uncertainty in m_{sat} is an order of magnitude smaller than the 10% uncertainty from the film thickness.

Previous studies of bulk polycrystalline NdN also show m_{sat} smaller than the free-ion value, though still larger than the value we measure. Schumacher and Wallace [17] reported $m_{\text{sat}} = 2.15\mu_B$ for powder NdN at 2 K. Other studies reported similarly high values between 1.8 and $3.1\mu_B$ (see Table I). It should be noted that the pulsed field experiments providing $3.1\mu_B$ were not considered reliable, since they make use of an extrapolation procedure [19,35], such that $2.7\mu_B$ [22] is likely the highest reported value of significance. In any case, it becomes clear that the ferromagnetic moment in NdN is reduced compared to the free-ion value of $3.27\mu_B$. The reduced ferromagnetic moment in NdN has been discussed in the literature before, but could not be sufficiently explained by crystal field calculations [22,35], especially since early experimental techniques provided limited knowledge about the crystal field splitting level scheme. A reduced ferromagnetic moment has also been observed for SmN. Our recent study explains the reduced SmN moment by performing calculations

that take the J admixture and crystal field effects into account [36]. In the next section we use the same method with some modifications to explain the reduced moment in NdN.

C. Calculations of the NdN moment in a crystal field approach

The ground-state moment of NdN can be calculated using a crystal field approach outlined in Refs. [37,38], which is similar to the well-known Steven's method, but also incorporates the effects of J mixing, which is most significant in Sm and Eu compounds but still non-negligible in NdN. In this approach, an effective $4f$ Hamiltonian with terms including the spin-orbit coupling (\mathcal{H}_{SO}), exchange in a mean-field approach (\mathcal{H}_{ex}), and the crystal field (\mathcal{H}_{CF}) representing the effect of the nitrogen anions is diagonalized using a self-consistent approach for the exchange energy, allowing for calculation of the ground-state $4f$ moment. Details of the calculation method are given in Refs. [36,39]. The parameters suitable for NdN are given by a spin-orbit coupling constant of $\Lambda = 500$ K [40], and an exchange constant derived from θ_p in the mean-field approximation; $\mathcal{J} = \frac{3}{2}k_B\theta_p/G$, where $G = (g_j - 1)^2 J(J + 1)$ is the de Gennes factor.

The crystal-field term is chosen with the z axis in the [100] direction, which yields the lowest energy ground state when compared to the [111] and [110] directions, and is given in Ref. [37]. The matrix elements of \mathcal{H}_{CF} depend on the fourth- and sixth-order crystal-field parameters $A_4\langle r^4 \rangle$ and $A_6\langle r^6 \rangle$. We use the point-charge model to estimate the parameters A_4 and A_6 , with nonrelativistic Hartree-Fock values used for $\langle r^4 \rangle$ and $\langle r^6 \rangle$ [41]. In the point-charge model, the crystal-field parameters are given by

$$A_4 = \frac{7}{16} \frac{Ze^2}{R^5}, \quad A_6 = \frac{3}{64} \frac{Ze^2}{R^7}, \quad (2)$$

where $R = a/2$ is half the NdN lattice constant, and Z is a phenomenological effective charge parameter. For the light rare-earth pnictides (P, As, Sb, and Bi), which are metallic, values of $Z \approx 2$ describe the trend in crystal-field parameters derived from neutron scattering [42]. In the semiconducting nitrides, larger values of Z have been observed, from 2.8 to 4.2 [20], though no systematic studies have been carried out.

Table II shows the ground-state ferromagnetic NdN moment $m_{\text{net}} = -\mu_B\langle L_z + 2S_z \rangle$ for $Z = 3$ for different θ_p and therefore different exchange constants \mathcal{J} . Good agreement is found between the historical data in Table I with m_{sat} between 1.8 and $2.7\mu_B$ and the moment calculated using a cubic crystal field and θ_p in the measured range between 5 and 25 K. However, the present thin-film data, with small moments close to $1\mu_B$ and weak exchange, fit much better with a model which incorporates a tetragonal stretching of the unit cell which we chose here as $\epsilon = \Delta R/R = 0.002$. This small tetragonal distortion can be accounted for by adding a second-order crystal-field term with strength $A_2\langle r^2 \rangle = -3\epsilon Ze^2/R^3$ [43]. A distortion of that magnitude could easily arise from the difference in thermal expansion between the substrate and the film, given that between the growth and the measurement temperatures the sample is cooled by several hundred Kelvin. Altered magnetic moments caused by lattice strain have been observed before for $3d$ and $4d$ transition-metal

TABLE II. Calculated values of the NdN ground-state moments with crystal-field parameters given in the point-charge model, with effective charge $Z = 3$ and with the exchange constant estimate from $\mathcal{J} = \frac{3}{2}k_B\theta_p/G$. The distorted crystal field is due to a tetragonal stretching of the unit cell.

Crystal field	Z	θ_p (K)	$m_{\text{net}} (\mu_B)$	$m_L (\mu_B)$	$m_S (\mu_B)$
Cubic	3	5	1.55	2.73	-1.18
Cubic	3	15	2.35	4.19	-1.84
Cubic	3	25	2.89	5.21	-2.32
Distorted	3	5	0.87	1.51	-0.64
Distorted	3	10	0.97	1.69	-0.72

Crystal-field parameters			
Z	A_2 (K) ^a	A_4 (K)	A_6 (K)
3	-49.86	370.6	8.7

^aWith $\epsilon = 0.002$.

systems [44–46]. A tetragonal distortion was chosen because some rare-earth pnictides, among them NdSb, were found to form a tetragonal phase at low temperatures [43]. At this stage we can only show that a small distortion from the cubic phase can account for the significant reduction of the ferromagnetic moment in NdN thin films. The tetragonal distortion of the given magnitude is just one possible choice; the distortion causing the reduced moment might also be of a different kind, e.g., trigonal. Detailed low temperature studies will need to be performed to determine the exact nature of the distortion, but based on the present data we can conclude that lattice strain is responsible for the relatively small ferromagnetic moment measured in NdN films.

The calculations also reveal that, like in SmN, the orbital moment m_L in NdN is larger than the spin moment m_S , which means the net magnetic moment points into the direction of the orbital moment. In contrast to SmN, in NdN the orbital moment is about twice as large as the spin moment, resulting in a strong

orbital-dominant magnetism. Experimental evidence for this spin/orbital moment alignment is given in the next section.

D. Spin/orbital magnetic moment alignment

The magnetization results in Sec. III B serve to determine the total magnetic moment in NdN, but to investigate the spin vs orbital dominance we turn to XMCD at the Nd $L_{2,3}$ edges. In Fig. 6 we show the XAS and XMCD spectra taken on a NdN thin film at 16 K in a magnetic field of 1.2 T, after field cooling in the same field of 1.2 T. These access the spin/orbital alignment of the $5d$ shell of Nd, so for determining the $4f$ shell spin alignment we rely on the ferromagnetic $4f$ - $5d$ exchange interaction. It is well established that rare-earth $L_{2,3}$ XMCD does not conform to the usual sum rules permitting a separate determination of $5d$ spin and orbit, most notably because the $4f$ - $5d$ exchange interaction drives a contraction of the majority spin $5d$ wave function [47]. Thus we rely on a simpler interpretation, so that to the first approximation the XMCD spectrum represents a spin splitting in the $5d$ states. Within this approximation the XMCD signal follows the derivative of the XAS spectrum, with a strength and sign that relates directly to the spin splitting. Thus we note that the signs of the XMCD spectra shown in Fig. 6 are opposite to those of GdN [48], and the same as SmN [4], signaling that the $4f$ magnetic moment is dominated by the orbital contribution. Figure 6(a) also shows an electric quadrupole (EQ) signal below the L_3 edge from the $2p \rightarrow 4f$ transition. A relatively strong EQ signal is commonly observed at the L_3 edge of the light rare earths, where the electric dipole signal is relatively weak [4,47].

Figure 6 also displays the calculated spectra as obtained from LSDA + U calculations. The calculations were scaled to achieve quantitative agreement with the experimental data. The XAS spectra are in good agreement, but the XMCD spectra show an opposing sign between the calculated and measured spectra, which again provides evidence for an orbital-dominated magnetic moment in NdN, as we explain below.

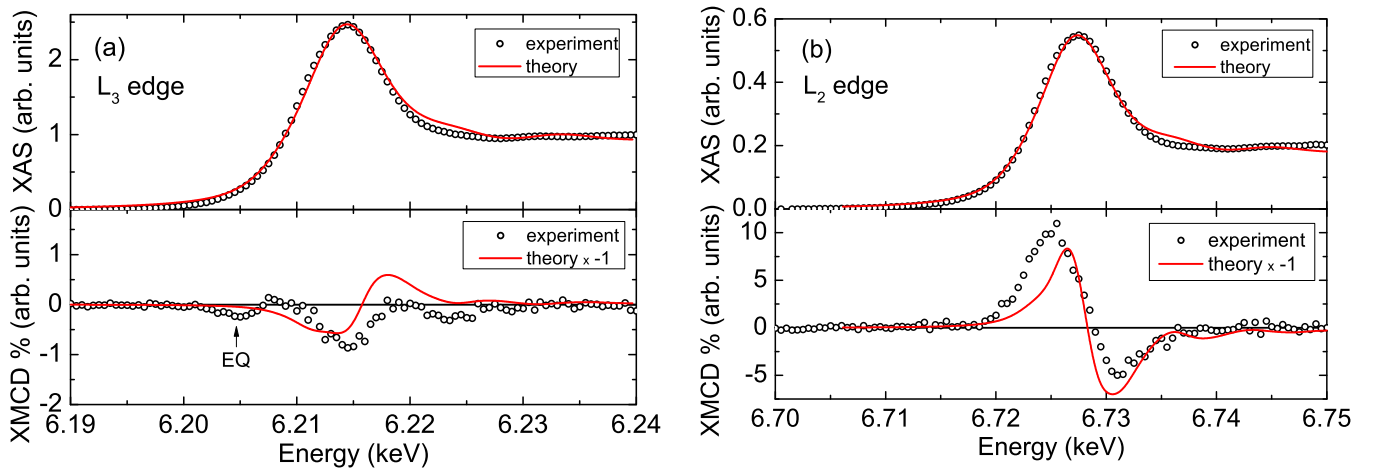


FIG. 6. XAS and XMCD of the (a) Nd L_3 and (b) L_2 edges, measured at 16 K in 1.2 T. The NdN film was grown on a sapphire substrate and capped with AlN. The red lines represent the XAS and XMCD obtained from a LSDA + U calculation. In the case of the XMCD, the calculated spectra were inverted for easier comparison of the features. The sign difference between experimental and calculated spectra provides evidence of an orbital dominated net magnetic moment (see text for details).

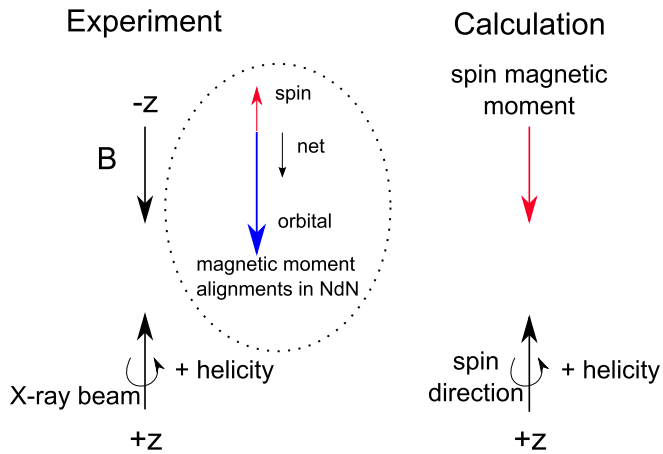


FIG. 7. Sketch of sign conventions in XMCD experiments and calculations, including a schematic of the alignment of magnetic moments of NdN in a magnetic field.

The sign of the XMCD follows different conventions for experiments and calculations, as depicted in Fig. 7. In experiments, the positive $+z$ direction is the direction of the photon wave vector or the direction of the incoming x-ray beam, while the positive magnetic field B is applied in the $-z$ direction. The XMCD spectrum ΔI is then the difference between the XAS spectra taken with positive I^+ and negative helicity photons I^- , $\Delta I = I^+ - I^-$ [47]. For the calculations the spin direction is set along the $+z$ direction, the same axis along which the helicity of the photons is defined. This axis coincides with the direction of the x-ray beam in experiments. The spin magnetic moment is then along the $-z$ direction, which coincides with the direction of the positive magnetic field B in experiments. The sign difference between the experimental and calculated XMCD spectra then indicates that the spin magnetic moment of NdN in the experiment is aligned opposite to the direction assumed by the calculations. That means the spin magnetic moment points into the $+z$ direction, opposing the magnetic field. This again can be explained by a larger orbital contribution, which is antialigned to the spin magnetic moment. Since the orbital magnetic moment is dominant, the net magnetic moment aligns with the orbital contribution and with the magnetic field, leaving the spin magnetic moment aligned antiparallel to the field. The alignment of the spin and orbital contributions of the magnetic moment along with the net magnetic moment are also illustrated in Fig. 7.

IV. CONCLUSIONS

The transport, optical, and magnetic properties of NdN thin films grown by molecular beam epitaxy were investigated. Resistivity measurements show behavior typical for a heavily doped semiconductor or semimetal, with the measured optical band gap of about 0.9 eV providing further evidence for the semiconducting nature of NdN. The magnetic susceptibility of the NdN thin films at high temperature follows Curie-Weiss behavior with a Hund's rule paramagnetic moment, but deviates from this behavior at low temperatures due to crystal-field effects. Furthermore, the crystal field is shown to suppress the ferromagnetic moment to $1.0\mu_B$ in NdN thin films, compared to the ferromagnetic free-ion moment of $3.27\mu_B$ as well as historic bulk NdN moments between 1.8 and $2.7\mu_B$. The crystal-field calculations show that small distortions from the cubic phase can account for the small measured moment, such that lattice strain by thermal expansion mismatch is likely the cause for the suppressed ferromagnetic moment in NdN thin films. The 43 K T_C in the NdN thin films is also enhanced relative to the 27.6 to 35 K T_C 's found for bulk NdN. The coercive field of NdN is large, at 1.4 T, pointing towards applications as a hard ferromagnetic material in magnetic heterostructures combining soft and hard layers, such as magnetoresistive random-access memory devices. XMCD measurements demonstrated that the orbital magnetic moment dominates the net magnetic moment. These findings put NdN in the same class as SmN, which also has an orbital dominant ferromagnetic moment, though it is some 30 times smaller than the $1\mu_B$ moment observed in NdN thin films. The large, orbital-dominant ferromagnetic moment occurring in NdN thin films makes it an ideal material for studying orbital-driven magnetic phenomena, and should also provide an excellent material for integration within magnetic heterostructures.

ACKNOWLEDGMENTS

We acknowledge financial support from the NZ FRST (New Economy Research Fund). The MacDiarmid Institute is supported by the New Zealand Centres of Research Excellence Fund. E.A. thanks the Alexander von Humboldt Foundation and the MacDiarmid Institute for support through fellowships. We thank A. E. Pantoja for assistance with the XRR measurements. The synchrotron radiation experiments were performed at the BL39XU beamline of SPring-8 with the approval of the Japan Synchrotron Radiation Research Institute (JASRI) (Proposal No. 2014B1310).

- [1] F. Natali, B. J. Ruck, N. O. V. Plank, H. J. Trodahl, S. Granville, C. Meyer, and W. R. L. Lambrecht, *Prog. Mater. Sci.* **58**, 1316 (2013).
- [2] A. Kumar and S. Yusuf, *Phys. Rep.* **556**, 1 (2015).
- [3] C. Meyer, B. J. Ruck, J. Zhong, S. Granville, A. R. H. Preston, G. V. M. Williams, and H. J. Trodahl, *Phys. Rev. B* **78**, 174406 (2008).
- [4] E.-M. Anton, B. J. Ruck, C. Meyer, F. Natali, H. Warring, F. Wilhelm, A. Rogalev, V. N. Antonov, and H. J. Trodahl, *Phys. Rev. B* **87**, 134414 (2013).
- [5] P. Larson, W. R. L. Lambrecht, A. Chantis, and M. van Schilfgaarde, *Phys. Rev. B* **75**, 045114 (2007).
- [6] J. F. McNulty, E.-M. Anton, B. J. Ruck, F. Natali, H. Warring, F. Wilhelm, A. Rogalev, M. M. Soares, N. B. Brookes, and H. J. Trodahl, *Phys. Rev. B* **91**, 174426 (2015).
- [7] S. Granville, B. J. Ruck, F. Budde, A. Koo, D. J. Pringle, F. Kuchler, A. R. H. Preston, D. H. Housden, N. Lund, A. Bittar, G. V. M. Williams, and H. J. Trodahl, *Phys. Rev. B* **73**, 235335 (2006).

- [8] C. Meyer, B. J. Ruck, A. R. H. Preston, S. Granville, G. V. M. Williams, and H. J. Trodahl, *J. Magn. Magn. Mater.* **322**, 1973 (2010).
- [9] M. Azeem, B. J. Ruck, B. D. Le, H. Warring, H. J. Trodahl, N. M. Strickland, A. Koo, V. Goian, and S. Kamba, *J. Appl. Phys.* **113**, 203509 (2013).
- [10] A. R. H. Preston, S. Granville, D. H. Housden, B. Ludbrook, B. J. Ruck, H. J. Trodahl, A. Bittar, G. V. M. Williams, J. E. Downes, A. DeMasi, Y. Zhang, K. E. Smith, and W. R. L. Lambrecht, *Phys. Rev. B* **76**, 245120 (2007).
- [11] J. H. Richter, B. J. Ruck, M. Simpson, F. Natali, N. O. V. Plank, M. Azeem, H. J. Trodahl, A. R. H. Preston, B. Chen, J. McNulty, K. E. Smith, A. Tadich, B. Cowie, A. Svane, M. van Schilfgaard, and W. R. L. Lambrecht, *Phys. Rev. B* **84**, 235120 (2011).
- [12] H. Warring, B. J. Ruck, J. F. McNulty, E.-M. Anton, S. Granville, A. Koo, B. Cowie, and H. J. Trodahl, *Phys. Rev. B* **90**, 245206 (2014).
- [13] N. Sclar, *J. Appl. Phys.* **35**, 1534 (1964).
- [14] G. Busch, E. Kaldis, E. Schaufelberger-Teker, and P. Wachter, *Colloq. Int. C. N. R. S.* **180**, 359 (1970).
- [15] G. Busch, P. Junod, F. Levy, A. Menth, and O. Vogt, *Phys. Lett.* **14**, 264 (1965).
- [16] G. Busch, *J. Appl. Phys.* **38**, 1386 (1967).
- [17] D. P. Schumacher and W. E. Wallace, *Inorg. Chem.* **5**, 1563 (1966).
- [18] G. L. Olcese, *J. Phys. F: Met. Phys.* **9**, 569 (1979).
- [19] P. Junod, A. Menth, and O. Vogt, *Phys. kondens. Materie* **8**, 323 (1969).
- [20] F. Hulliger, *Handbook on the Physics and Chemistry of Rare Earths*, edited by J. K. A. Gschneidner and L. Eyring (North-Holland, New York, 1979), Vol. 4, pp. 153–236.
- [21] J. J. Veyssie, J. Chaussy, and A. Berton, *Phys. Lett.* **13**, 29 (1964).
- [22] P. Schobinger-Papamantellos, P. Fischer, O. Vogt, and E. Kaldis, *J. Phys. C* **6**, 725 (1973).
- [23] O. K. Andersen, *Phys. Rev. B* **12**, 3060 (1975).
- [24] V. Antonov, A. Perlov, A. Shpak, and A. Yaresko, *J. Magn. Magn. Mater.* **146**, 205 (1995).
- [25] V. I. Anisimov, J. Zaanen, and O. K. Andersen, *Phys. Rev. B* **44**, 943 (1991).
- [26] V. N. Antonov, V. P. Antropov, B. N. Harmon, A. N. Yaresko, and A. Y. Perlov, *Phys. Rev. B* **59**, 14552 (1999).
- [27] V. N. Antonov, B. N. Harmon, A. Y. Perlov, and A. N. Yaresko, *Phys. Rev. B* **59**, 14561 (1999).
- [28] F. Leuenberger, A. Parge, W. Felsch, K. Fauth, and M. Hessler, *Phys. Rev. B* **72**, 014427 (2005).
- [29] F. Natali, B. J. Ruck, H. J. Trodahl, D. L. Binh, S. Veziar, B. Damilano, Y. Cordier, F. Semond, and C. Meyer, *Phys. Rev. B* **87**, 035202 (2013).
- [30] F. Natali, N. O. V. Plank, J. Galipaud, B. J. Ruck, H. J. Trodahl, F. Semond, S. Sorieul, and L. Hirsch, *J. Cryst. Growth* **312**, 3583 (2010).
- [31] C. Mourgout, B. Chevalier, J. Étourneau, J. Portier, P. Hagemmuller, and R. Georges, *Rev. int. Htes Temp. et Réfract.* **14**, 89 (1977).
- [32] K. R. Lea, M. J. M. Leask, and W. P. Wolf, *J. Phys. Chem. Solids* **23**, 1381 (1962).
- [33] H. R. Child, M. K. Wilkinson, J. W. Cable, W. C. Koehler, and E. O. Wollan, *Phys. Rev.* **131**, 922 (1963).
- [34] H. L. Huang and M. Y. Lin, *Phys. Status Solidi A* **91**, 123 (1985).
- [35] A. Furrer and W. Hälg, *J. Phys. C* **9**, 3499 (1976).
- [36] J. F. McNulty, B. J. Ruck, and H. J. Trodahl, *Phys. Rev. B* **93**, 054413 (2016).
- [37] H. De Wijn, A. Van Diepen, and K. Buschow, *Phys. Status Solidi B* **76**, 11 (1976).
- [38] H. Adachi, H. Ino, and H. Miwa, *Phys. Rev. B* **56**, 349 (1997).
- [39] J. F. McNulty, Ph.D. thesis, Victoria University of Wellington, 2015.
- [40] J. Jensen and A. R. Mackintosh, *Rare Earth Magnetism* (Clarendon, Oxford, 1991).
- [41] A. J. Freeman and R. E. Watson, *Phys. Rev.* **127**, 2058 (1962).
- [42] R. J. Birgeneau, E. Bucher, J. P. Maita, L. Passell, and K. C. Turberfield, *Phys. Rev. B* **8**, 5345 (1973).
- [43] F. Lévy, *Phys. kondens. Materie* **10**, 71 (1969).
- [44] M. Björck, M. Pärnaste, M. Marcellini, G. Andersson, and B. Hjörvarsson, *J. Magn. Magn. Mater.* **313**, 230 (2007).
- [45] K. Ishigami, K. Yoshimatsu, D. Toyota, M. Takizawa, T. Yoshida, G. Shibata, T. Harano, Y. Takahashi, T. Kadono, V. K. Verma, V. R. Singh, Y. Takeda, T. Okane, Y. Saitoh, H. Yamagami, T. Koide, M. Oshima, H. Kumigashira, and A. Fujimori, *Phys. Rev. B* **92**, 064402 (2015).
- [46] S. I. Csiszar, M. W. Haverkort, Z. Hu, A. Tanaka, H. H. Hsieh, H.-J. Lin, C. T. Chen, T. Hibma, and L. H. Tjeng, *Phys. Rev. Lett.* **95**, 187205 (2005).
- [47] J. Parlebas, K. Asakura, A. Fujiwara, I. Harada, and A. Kotani, *Phys. Rep.* **431**, 1 (2006).
- [48] F. Leuenberger, A. Parge, W. Felsch, F. Baudalet, C. Giorgetti, E. Dartyge, and F. Wilhelm, *Phys. Rev. B* **73**, 214430 (2006).